Towards a Multi-legged Mobile Manipulator

Bilal Ur Rehman, Michele Focchi, Jinoh Lee, Houman Dallali, Darwin G. Caldwell and Claudio Semini

***Abstract*— A common disadvantage of multi-legged robots is that they often lack the manipulation capability. To overcome this limitation, an arm can be added to the body of the multi-legged robot, to perform manipulation tasks and provide assistance for locomotion. First, we proposed an attachment configuration of the arm for a multi-legged robot that provide a uniform workspace in front, below and above the base robot trunk. Second, an integrated control framework promises to keep the mobility and the balance of the mobile platform and provides precise manipulation capability of the arm incorporating a payload estimation scheme. Finally, we verify an integrated control framework with experimental results of a static and walking mobile platform while moving the arm.**

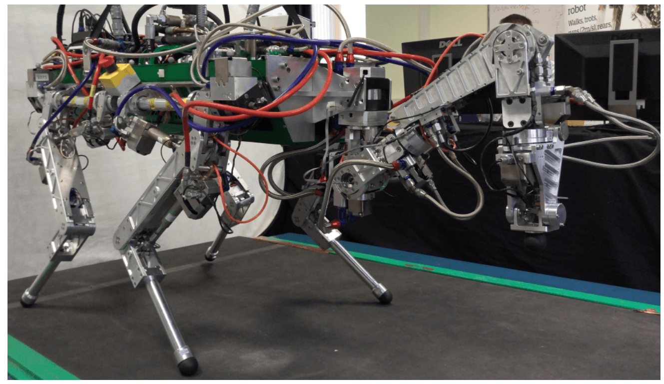

Fig. 1. Picture of IIT's HyQ robot [1] with the new hydraulic manipulator [4] attached to its front creating a multi-legged mobile manipulator.

I. Introduction

In the field of legged robots, bipeds and quadruped robots are the most popular among researchers. Quadruped robots have the advantage (over bipeds) of improved locomotion stability over rough terrain. However, a common disadvantage of a quadruped is that they are often limited to load carrying or inspection tasks due to their lack of manipulation capability. The Hydraulic Quadruped robot HyQ [1] was developed at IIT to traverse complex and unstructured terrain for search and rescue missions in natural disaster scenarios. HyQ has already shown a wide range of abilities such as trotting, running, jumping and navigation over unstructured terrain [2], [3]. However, similar to other quadruped robots HyQ lacks a manipulation ability. Indeed, a combination of quadruped locomotion stability with the ability to perform manipulation tasks can be crucial in natural disasters scenarios.

This paper presents a "best-of-both-worlds" approach by integrating a fully torque control hydraulic arm [4] with HyQ, thus creating a multi-legged mobile manipulator. This combination enables to perform new tasks, including: balance assistance, door opening, debris removal, grasping and object manipulation.

On the other hand, the integration of the arm, opens new challenges such as: what is the optimal mounting position of the arm on the mobile platform? When the integrated arm interacts with the environment or carries an unknown payload, a fundamental issue arises because the Center of Mass (CoM) of the whole robot can be dramatically shifted and the overall robot balance can be affected. How to maintain the mobility and balance of the quadruped robot? In addition to this, for precise object manipulation it is important that the arm controller is robust against external/internal disturbances (payload variation and unknown dynamics such as friction and inertial forces coming from the mobile base). This requires a suitable control scheme which is robust to disturbances and uncertainties coming from the robot dynamics and environment.

The contribution of this work is two-fold. First, we propose an attachment configuration of the arm to a multi-legged robot to provide a uniform workspace in front, below and above the base robot trunk, which is suitable for our required application. Second, a control framework that integrates the mobile platform controller with a robust model-free arm controller is presented. The mobile platform controller stabilizes the CoM position and the robot trunk orientation while optimizing for the Ground Reaction Forces (GRFs). The model-free arm controller estimates and compensates external/internal disturbances while tracking a joint desired trajectory, combined with a payload estimation scheme. We carried out experiments on a multi-legged mobile robot as shown in Fig. 1.

The article is organized as follows. Section II gives a brief literature review on multi-legged mobile manipulators. Section III presents an overview of the system and of its integration. Section IV describes the mobile platform controller. Section V presents a robust model-free arm controller and a payload estimation module to update location of the CoM. In Section VI we present experimental results that show the effectiveness of the proposed integrated control framework. Finally, Section VII draws the conclusions and presents future work directions.

II. Related work

The first known multi-legged mobile manipulator was AQUAROBOT in 1990 [5]. This robot was developed to

The authors are with Department of Advanced Robotics, Istituto Italiano di Tecnologia, via Morego, 30, 16163 Genova, Italy. `<bilal.rehman, michele.focchi, jinoh.lee, houman.dallali, darwin.caldwell, claudio.semini>@iit.it`

*This work is supported by Department of Advanced Robotics, Istituto Italiano di Tecnologia, via Morego, 30, 16163 Genova, Italy.

carry out underwater inspecting works. The AQUAROBOT has six legs to walk underwater at a $50m$ depth and is equipped with a TV camera and ultrasonic ranging device at the end of a manipulator mounted on the mobile platform.

In the same period, the first known centaur-like[1] robot (electrically actuated) was developed by the Advanced Robotics Technology Research Association Japan [6]. A few years later, a similar robot was developed by the Humanoid Robot Research Center and KIST Korea [7]. The Korean centaur robot stood $1.8m$ tall and weighed $150kg$ with hydraulically actuated legs and electric upper body. These robot were developed as nuclear inspection machines.

Tsuda et al. presented a research on a small centaur-like robot that was actuated by electric DC servo motors in 2007 [8]. Several other centaur-style robots were developed with wheels at the end of their legs (e.g. WorkPartner [9], NASA centaur 2, NimbRo [10]). There are also hexapod robots which use their legs as arms to perform manipulation tasks, such as the LAURON V [11].

BigDog (with an arm attached) from Boston Dynamics was shown throwing a cinder block [12]. They combined robot body, legs and arm to improve strength, velocity of the trowing motion and increase the workspace. They provided off-line optimized planned trajectories for two decoupled trot and arm controllers to perform a throwing task. The off-line trajectory generator planned the foot location and the body forces while satisfying physical constraints, namely the center of pressure location, joint torques, speed and kinematic limits.

Recently, Hutter et al. [13] presented an article on walking excavators. They proposed an optimal force distribution method to keep center of mass inside the support triangle and to level the cabin while performing excavation/locomotion.

III. System overview

This section presents an overview of the mobile platform, the manipulator, and shows how they were integrated.

A. The mobile platform

HyQ is a fully torque-controlled hydraulically actuated 12 Degree-of-Freedom (DoF) quadruped robot [1]. HyQ weighs $80kg$, is roughly $1m$ long and has a leg length of $0.78m$ (fully stretched). Each leg has three degrees of freedom: the hip abduction/adduction (HAA), hip flexion/extension (HFE) and the knee flexion/extension (KFE). The legs are actuated by a combination of hydraulic motors and cylinders. In addition, HyQ has an on-board *inertial measurement unit* (IMU), position, torque/force sensors, and an on-board 4-core computer.

B. The manipulator

We developed a fully torque-controlled and **Hy**draulically actuated **Arm** (HyArm) [4] (see Fig. 2), tailored for a $80kg$ quadruped robot (HyQ). The arm was designed to be compact, light-weight ($12.5kg$) and able to carry a heavy payload ($10kg$ in the entire workspace, when attached to a fixed base).

[1]The Centaur is a mythological creature with the upper body of a human and lower body of a horse.

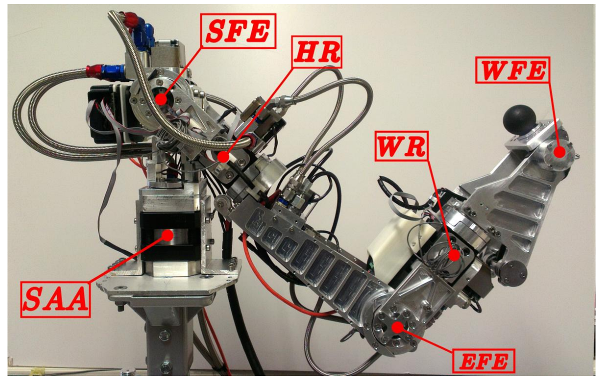

Fig. 2. The HyArm: A fully torque-controlled **Hy**draulic **A**rm with joint names: Shoulder Adduction/Abduction (SAA), Shoulder Flexion/Extension (SFE), Humerus Rotation (HR), Elbow Flexion/Extension (EFE), Wrist Rotation (WR), Wrist Flexion/Extension (WFE).

TABLE I
Manipulator joint specifications

Joint	**Range of motion**[rad]	**Torque**[Nm]
SAA	-1.57 to 0.52	126
SFE	-0.74 to 0.83	120
HR	-1.598 to 0.068	120
EFE	0 to 2.21	225
WR	-2.08 to 1.57	60
WFE	-0.52 to 1.57	100

The HyArm has six actuated joints and DoFs with a combination of rotary and linear hydraulic actuators. The HyArm shoulder joints, adduction/abduction (SAA), flexion/extension (SFE) and humerus rotation (HR) are equipped with rotary motors to improve compactness that keeps the CoM of the arm closer to the arm base. The elbow flexion/extension (EFE) joint is actuated by a hydraulic cylinder. This choice has the advantage that the whole elbow assembly is part of the upper arm. The wrist joints play an important role in determining end-effector position and orientation. For the wrist rotation WR joint we selected a rotary actuator to achieve a wider range of motion (Table. I). Finally, the wrist flexion/extension WFE joint is actuated by a cylinder. The HyArm is also equipped with position encoders and torque/force sensors to achieve torque control.

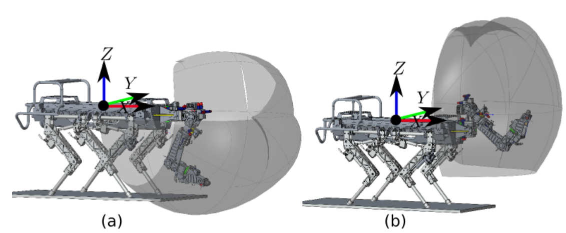

Fig. 3. Sketch of the arm 3D workspace in an elbow-down configuration, with the arm base: rotated 90[deg] (a) or aligned (b) with the mobile base Z-axis.

C. System integration

The manipulator can be attached to the front-middle of the HyQ either in a elbow-down or elbow-up configuration. The placement of arm in front-middle has the advantage that

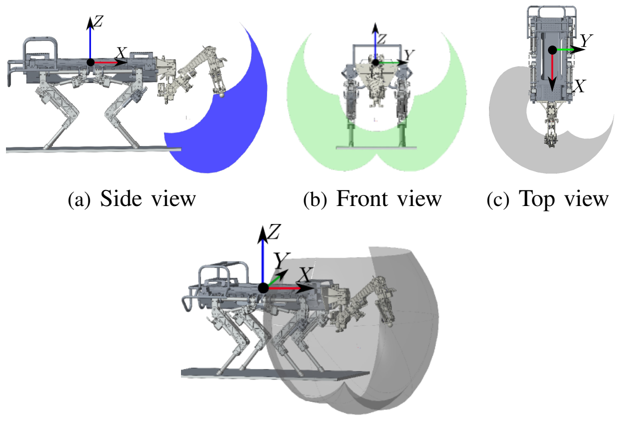

(a) Side view (b) Front view (c) Top view

(d) 3D view

Fig. 4. 2D views of the arm workspace in an elbow-up configuration with the arm base rotated 180$[deg]$ w.r.t X-axis of the mobile base frame: (a) X-Z plane, (b) Y-Z plane, (c) X-Y plan. (d) 3D view.

the weight of the arm is shared by both front legs, but the disadvantage is that the weight distribution of the mobile platform gets unbalance [2]. Given the arm joint range of motion limitation (see Table I), we considered three different attachment configurations as shown in Fig. 3 and 4. The elbow-down configuration with the arm base link rotated at (a) 90$[deg]$ and (b) aligned to the Z-axis of the mobile base are shown in Fig. 3. In (a) the arm workspace partially overlaps with only the front left leg. This configuration provided ground reachability, but there is a inconsistency between left and right sides of the mobile platform. Whereas in (b) a larger workspace in front and above the trunk. However this configuration does not provide a possibility to perform tasks such as balance assistance (acting as fifth leg) or debris removal from the ground. On the other hand, the elbow-up configuration shown in Fig. 4 (the arm base link is rotated at 180$[deg]$ w.r.t mobile robot X-axis) allows the manipulator to achieve a uniform workspace in front, below and above the base robot trunk. We selected this configuration because the manipulator can be used to provide balance assistance for locomotion by acting as a fifth leg or perform manipulation tasks as mentioned earlier.

IV. Mobile platform controller with optimization of the ground reaction forces

In this section, we present the algorithm used for controlling the CoM position and robot trunk orientation while optimizing for the ground reaction forces (GRFs). The arm placement shifts the CoM significantly, requiring an algorithm which redistributes the load on the stance feet to maintain the balance. For control purposes we applied a linear mapping between GRFs and robot body accelerations using a lower dimensional model of the robot (massless legs) which takes into account only the centroidal dynamics.

A. Centroidal robot dynamics

We assume the GRFs are the only external forces acting on the system. Therefore, we can express the linear acceleration

[2]In Section IV and V, we will address this problem in detail and provide an optimal solution.

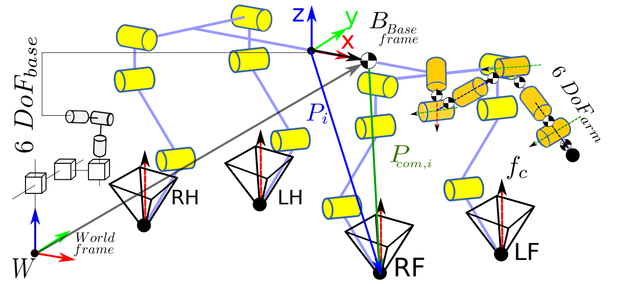

Fig. 5. Summary of the nomenclature used in the paper. Leg labels: left front (LF), right front (RF), left hind (LH) and right hind (RH). The world frame W, the base frame B (attached to the geometric center of the robot body). Left subscripts indicate the reference frame, for instance $B^{x_{com}}$ is the location of the *CoM* w.r.t. the base frame. In case of no left subscript, quantities are expressed w.r.t. W. The C_i is i^{th} contact point between ground and i^{th} limb. The f_c is the ground reaction force (GRFs), where c is the number of stance feet.

of the CoM $\ddot{x}_{com} \in \mathbb{R}^3$ and the angular acceleration of the base $\dot{\omega}_b$ as functions of the GRFs (i.e. $f_1, \ldots, f_c \in \mathbb{R}^3$, where c is the index of stance feet):

$$m(\ddot{x}_{com} + g) = \sum_{i=1}^{c} f_i \tag{1}$$

$$I_G \dot{\omega}_b \simeq \sum_{i=1}^{c} (p_{com,i} \times f_i), \tag{2}$$

where $m \in \mathbb{R}$ is the total robot's mass, $g \in \mathbb{R}^3$ is the gravity acceleration vector, $I_G \in \mathbb{R}^{3\times 3}$ is the centroidal rotational inertia [14], $p_{com,i} \in \mathbb{R}^3$ is a vector going from the CoM to the position of the i^{th} foot defined in an inertial world frame $\mathscr{W}$ (see Fig. 5). Since our platform has nearly point-like feet, we assume that it cannot generate moments at the contacts, thus f_c are pure linear forces. As a final remark the term $\dot{I}_G \omega_G$ in the Euler equation (2) was neglected. Indeed, even though the presence of the moving masses of the arm links can potentially create changes on I_G, we will only consider experiments which involves small ω_G, making the term $\dot{I}_G \omega_G$ very small. Equations (1) and (2) describe how the GRFs affect the CoM acceleration and the angular acceleration of the robot's base.

B. Control of CoM and base orientation

A *trajectory generation* module (see. Fig. 6) computes desired trajectories for the CoM, the base orientation the swing foot (e.g. to achieve a static walking pattern [15]). We compute the desired acceleration of the CoM $\ddot{x}^d_{com} \in \mathbb{R}^3$ and the desired angular acceleration of the robot's base $\dot{\omega}^d_b \in \mathbb{R}^3$ using a PD control law:

$$\ddot{x}^d_{com} = K_{pcom}(x^d_{com} - x_{com}) + K_{dcom}(\dot{x}^d_{com} - \dot{x}_{com}) \tag{3}$$

$$\dot{\omega}^d_b = K_{pbase} e(R^d_b R^\top_b) + K_{dbase}(\omega^d_b - \omega_b) \tag{4}$$

where $x^d_{com} \in \mathbb{R}^3$ is the desired position of the CoM, and $R^\top_b \in \mathbb{R}^{3\times 3}$ and $R^d_b \in \mathbb{R}^{3\times 3}$ are coordinate rotation matrices representing the actual and desired orientation of the base w.r.t. the world reference frame, respectively,

$e(\cdot) : \mathbb{R}^{3\times 3} \to \mathbb{R}^3$ is a mapping from a rotation matrix to the associated rotation vector, $\omega_b \in \mathbb{R}^3$ is the angular velocity of the base.

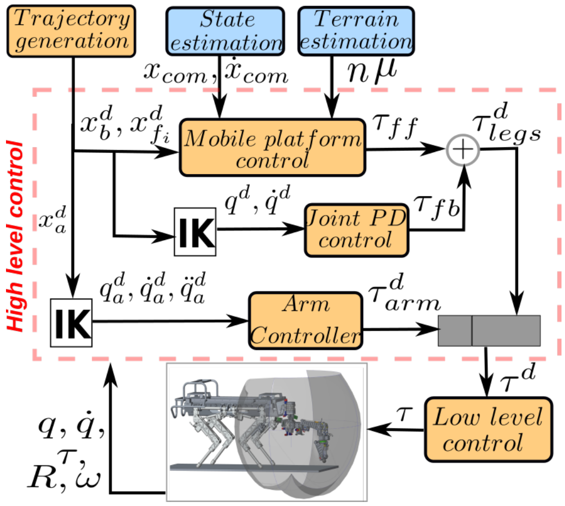

Fig. 6. Block diagram of the control framework. The trajectory generation block compute desired trajectories for the robot CoM, the base orientation and joints. The high level control computes the reference torques for the low-level controller. For further detail see Section IV and V.

C. Computation of desired GRFs

Given a desired value of the linear acceleration of the CoM and the angular acceleration of the robot's base it is possible to rewrite (1) and (2) in matrix form:

$$\underbrace{\begin{bmatrix} I & \dots & I \\ [p_{com,1}\times] & \dots & [p_{com,c}\times] \end{bmatrix}}_{A} \underbrace{\begin{bmatrix} f_1 \\ \cdot \\ \cdot \\ \cdot \\ f_c \end{bmatrix}}_{f} = \underbrace{\begin{bmatrix} m(\ddot{x}^d_{com} + g) \\ I_g \dot{\omega}^d_b \end{bmatrix}}_{b}, \quad (5)$$

The desired GRFs are computed every control loop by solving the following optimization problem as a quadratic program [15]:

$$\begin{aligned} f^d = & \underset{f \in \mathbb{R}^k}{\operatorname{argmin}} (Af - b)^\top S (Af - b) + \alpha f^\top W f \\ & \text{s.t.} \quad \underline{d} < Cf < \bar{d}, \end{aligned} \quad (6)$$

where $S \in \mathbb{R}^{6\times6}$ and $W \in \mathbb{R}^{k\times k}$ are positive-definite weight matrices, $\alpha \in \mathbb{R}$ weighs the secondary objective (e.g. regularization to keep the solution bounded), $C \in \mathbb{R}^{p\times k}$ is the inequality constraint matrix, $\underline{d}, \bar{d} \in \mathbb{R}^p$ the lower/upper bound respectively, with p being the number of inequality constraints. These ensure that a) the GRFs lie inside the friction cones and b) the normal components of the GRFs stay within some user-defined values. We exploit the redundancy of the solution to ensure the respect of these inequality constraints, and approximate friction cones with a square pyramid model to express them as linear constraints. The desired joint torques $\tau^d_{legs} \in \mathbb{R}^{n_{legs}}$ (where n_{legs} is the number of leg actuated joints) computed by superimposing two control actions. First, the mobile platform control block maps the desired GRFs f^d into joint space, outputting the feedforward torques τ_{ff}:

$$\tau_{ff} = -S_{legs} J_c^\top f^d, \quad (7)$$

where $J_c \in \mathbb{R}^{k\times n+6}$ is the stacked Jacobian of the contact points and S_{legs} is a selection matrix that selects the legs DoF. The same mapping was used by Ott et al. [16] and it is valid only for quasi-static motion. Second, the joint PD control block consists of a proportional-derivative (PD) joint-position controller with low gains motivated by safety reasons that hydraulic actuators can generate fast and powerful movements, and it is also used to move the swing leg. During the swing motion we increase the PD gains of the swing leg joints to improve tracking capabilities. The desired arm torques τ^d_{arm} are computed as described in Section V. The whole vector of desired torque $\tau^d = \begin{bmatrix} \tau^{d\ T}_{legs} & \tau^{d\ T}_{arm} \end{bmatrix}^T$ is then sent to the underlying joint-torque controllers (see Fig 6) [17].

V. Arm Controller

As a first step in the development of the arm controller, it is useful to evaluate the influence that the quadrupedal mobile platform has on the arm dynamics. Differently from Section IV-A where we used a simplified model, here we will consider the full floating base model of the robot.

A. Dynamics of a floating-base system

The dynamics of a floating-base articulated-body system can be expressed as two coupled dynamics equations: the one of the floating-base body (6 DoFs underactuated) and the one of the n rigid-bodies attached to it. In the case of the our robot we have 5 kinematic branches: 4 legs and 1 arm, thus $n = n_{legs} + n_{arm}$. The equation of motions of such a system can be partitioned as follows [18]:

$$\left[\begin{array}{c|c} I^c_0 & F \\ \hline F^T & M \end{array}\right] \begin{bmatrix} a_0 \\ \ddot{q} \end{bmatrix} + \begin{bmatrix} h^c_0 \\ h \end{bmatrix} = \begin{bmatrix} 0 \\ \tau \end{bmatrix}, \quad (8)$$

where $I^c_0 \in \mathbb{R}^{6\times6}$ is the composite rigid body inertia of the robot, $F \in \mathbb{R}^{6\times n}$ is a matrix which contains the spatial forces required at the floating base to support each joint variable, h^c_0 is the spatial bias force for the composite rigid body containing the whole floating-base system, $M \in \mathbb{R}^{n\times n}$ denotes active joints links (legs and arm) inertia matrix, $h \in \mathbb{R}^n$ denotes the correspondent vector of Coriolis, centrifugal and gravitational forces, $a_0 \in \mathbb{R}^6$ and $\ddot{q} \in \mathbb{R}^n$ denote floating-base and joint acceleration vectors respectively, and $\tau \in \mathbb{R}^n$ denote vector of joint torques and including the contribution of ground reaction forces. Starting with (8), we subtract $F^T (I^c_0)^{-1}$ times the first row from the second. The resulting equation is

$$\left[\begin{array}{c|c} I^c_0 & F \\ \hline 0 & M - F^T (I^c_0)^{-1} F \end{array}\right] \begin{bmatrix} a_0 \\ \ddot{q} \end{bmatrix} + \begin{bmatrix} h^c_0 \\ h - F^T (I^c_0)^{-1} h^c_0 \end{bmatrix} = \begin{bmatrix} 0 \\ \tau \end{bmatrix} \quad (9)$$

The bottom row from (9), can be decoupled as:

$$M^{fl} \ddot{q} + h^{fl} = \tau \quad (10)$$

where, $M^{fl} = M - F^T (I^c_0)^{-1} F$ and $h^{fl} = h - F^T (I^c_0)^{-1} h^c_0$. This equation provides a direct relation between $\ddot{q}$ and τ incorporating the inertia of the base. M^{fl} and h^{fl} can be regarded as floating-base analogues to the coefficients of the standard fixed-base dynamic equation. Equation (10) can be further subdivided as follows:

$$\left[\begin{array}{c|c} M_{11}^{fl} & M_{12}^{fl} \\ \hline M_{21}^{fl} & M_{22}^{fl} \end{array}\right]\left[\begin{array}{c} \ddot{q}_{n_{legs}} \\ \ddot{q}_{n_{arm}} \end{array}\right]+\left[\begin{array}{c} h_{n_{legs}}^{fl} \\ h_{n_{arm}}^{fl} \end{array}\right]=\left[\begin{array}{c} \tau_{n_{legs}} \\ \tau_{n_{arm}} \end{array}\right] \tag{11}$$

Extracting the bottom row from (11) we get:

$$M_{21}^{fl}\ddot{q}_{n_{legs}}+M_{22}^{fl}\ddot{q}_{n_{arm}}+h_{n_{arm}}^{fl}=\tau_{n_{arm}}. \tag{12}$$

Rearranging (12) and adding an external disturbance term τ_{ext},

$$\tau_{n_{arm}}=M_{22}^{fl}\ddot{q}_{n_{arm}}+M_{21}\ddot{q}_{n_{legs}}+h_{n_{arm}}^{fl}+\tau_{ext}, \tag{13}$$

presents a direct relation between $\ddot{q}_{n_{arm}}$, $\ddot{q}_{n_{legs}}$, external disturbance τ_{ext}, the influence of leg motion (internal disturbance) and $\tau_{n_{arm}}$. Equation (13) can only be used to develop model-based control schemes which require perfect knowledge of robot dynamics and disturbances. The robot dynamics non-linear terms are tightly coupled, and small model discrepancies can lead to instabilities. To avoid model estimation we choose a model-free control scheme based on time-delay estimation (TDE).

B. Time delay controller

The target of the arm controller is to compensate all external and internal disturbances such that the arm joints positions $q_{n_{arm}}$ can track a desired trajectory $q_{n_{arm}}^{d}$ in a robust way. To achieve this we adopt a time-delay estimation (TDE) scheme which provides a model-free control law to compensate for the non-linearities terms of robot dynamics and to enforce the desired dynamics for the tracking error.

Following a procedure similar to [19], we rearrange (13) and introduce a constant diagonal matrix $\overline{M}$, which may assume the nominal values of M_{22}^{fl}:

$$\tau_{arm}=(\overline{M}+M_{22}^{fl}-\overline{M})\ddot{q}_{n_{arm}}+M_{21}^{fl}\ddot{q}_{n_{legs}}+h_{n_{arm}}^{fl}+\tau_{ext}, \tag{14}$$

now we work-out the linear (decoupled) part and group all the non-linearities and couplings of the robot dynamics, internal and external disturbances into a vector H:

$$\tau_{n_{arm}}=\overline{M}\ddot{q}_{n_{arm}}+\underbrace{(M_{22}^{fl}-\overline{M})\ddot{q}_{n_{arm}}+M_{21}^{fl}\ddot{q}_{n_{legs}}+h_{n_{arm}}^{fl}+\tau_{ext}}_{H} \tag{15}$$

$$\tau_{n_{arm}}=\overline{M}\ddot{q}_{n_{arm}}+H \tag{16}$$

A model-free time delay controller designed for tracking joint position has the following structure:

$$\tau_{n_{arm}}^{d}=\overline{M}\upsilon+\hat{H}, \tag{17}$$

where υ represents the control input to the linear system ($\bar{M}$ is constant diagonal) and is defined as follows:

$$\upsilon=\ddot{q}_{n_{arm}}^{d}+K_{d_{n_{arm}}}\dot{e}_{n_{arm}}+K_{p_{n_{arm}}}e_{n_{arm}}, \tag{18}$$

where $e_{n_{arm}}$ is the tracking error between the actual $q_{n_{arm}}$ and the desired $q_{n_{arm}}^{d}$ arm joint position, $\hat{H}$ is an estimate of H and $K_{p_{n_{arm}}}$ and $K_{d_{n_{arm}}}$ are the proportional and derivative gains respectively. Next, we substitute (18) as the control input to (17). If $\hat{H}$ is a good estimate of H the tracking error converges to zero with a desired second-order dynamics set by $K_{d_{n_{arm}}}=2\omega_n\varsigma I_n$ and $K_{p_{n_{arm}}}=\omega_n^2 I_n$, where ω_n and ς are desired natural frequency and damping ratio, respectively.

From (16) it can be noticed that $H=\tau_{arm}-\overline{M}\ddot{q}_{arm}$. Due to a violation of causality we cannot use measurement data of τ and $\ddot{q}_{arm}$ at time t to compute H. In this respect the main idea of TDE is to use 1-sample delayed measurements for the estimation:

$$\hat{H}\approx\tau_{arm}(t-T_s)-\overline{M}\ddot{q}_{arm}(t-T_s) \tag{19}$$

where T_s is the sampling interval; for example, $T_s=1ms$ is used in this case study. Finally, we use (19) into (17) to obtain the torque command $\tau_{n_{arm}}^{d}$ that will compensate for external and internal disturbances and track the desired arm position trajectory. The stability condition of the time-delay controller is well-established by Youcef-Toumi [20] and Hsia [21], independently, represented as $||I-M_{22}^{fl^{-1}}\bar{M}||<1$.

C. Payload estimation

Payload estimation is an essential feature for our platform because the weight added by an object at the end of the arm can cause loss of stability if not properly accounted for.

In this section, we will present how we implemented this feature in our framework. We assume there are not relevant disturbance forces coming from the quadruped platform. In this respect, we treat the arm as a fixed base. Moreover we restrict the case of a point mass object rigidly attached to the arm tip (hand) leaving the generalization to the case of a rigid-body moving object to future works. The arm controller will compensate for the joint position tracking error generated by the added payload. The basic idea is to compare the arm torques predicted by the model with the real ones. Subsequently, mapping the resulting torque error vector to the force at the end effector through kinematics. Finally, the resulting wrench (6 Dofs) in the direction of gravity to identify the gravity (linear) force of the added mass.

$$\begin{aligned} {}_wF_m &= {}_wX_b^{*}J^{-T}(\tau_{ID}-\tau_{arm}) \\ m_p &= {}_wF_{m_z}/g \end{aligned} \tag{20}$$

where ${}_wF_m$ is the wrench at the end effector defined in the world frame, ${}_wX_b^{*}$ is a pure rotation spatial transform which maps the wrench from the base to the world frame. $J\in\mathbb{R}^{6\times6}$ is the Jacobian of the end-effector from the arm attachment to the end-effector (note that we use a standard inversion because Jacobian is a square matrix). τ_{ID} are the torques predicted by the model of the arm to stay in the actual configuration and τ_{arm} the measured torques. We used estimated payload m_p to update the CoM location to ensure the robot balance.

VI. Experiments

We carried out a set of experiments on the multi-legged mobile manipulator. We performed gradual assessment of the full system by dividing them into four different groups: (A) a static test with moving arm, to assess the capability of the mobile platform controller to regulate the CoM motion. Indeed the CoM moves due to the motion of the arm and to compensate for the unbalanced load caused by the weight of the arm. (B) Arm controller tracking, to assess the desired joint position tracking capabilities of the arm controller while compensating for gravity, friction and other disturbances. (C) Payload estimation while the mobile platform is standing still and the arm is carrying an unknown payload. (D) Walking tests with the arm moving, to verify the capability of both the arm and mobile controllers.

A. Static base with moving arm

Although the mobile platform controller for legs is decoupled from the arm, there is a significant influence from the arm motion. This can be dealt (damped) with the mobile platform controller, because we consider the contribution of the arm joints in the whole robot CoM computation and this is actively controlled in our framework. Fig. 8 shows the effectiveness of the mobile platform controller by comparing two scenarios, (a) when the mobile controller is actively damping disturbances coming from the arm motion by optimizing the GRF and (b) without optimization. We gave a sinusoidal trajectory as a reference to the arm SAA joint with an amplitude of $0.5rad$ and frequency at $0.7Hz$ as a disturbance source for the mobile platform. In Fig. 7 the first row shows effects of the arm motion the base robot torso is pitched forward and creating a big yaw motion compared to the second row with GRF optimization robot torso is stable and horizontal. We performed the various experiments with different frequencies, root-mean-square (RMS) value peak to peak oscillation on CoM Y are summarized in Table II. The enclosed video (see Section VIII) shows the experimental results with static base and moving arm.

B. Arm controller tracking

In this section, we show experimental results that demonstrate the ability of the TDE controller to reject gravity disturbances. For the sake of brevity we will only report the tracking of the three shoulder joints which are mostly affected by gravity and large inertia. As shown in Fig. 9, the desired trajectories are defined by a sinusoidal function with different frequencies for each joint. Despite the absence of any kind of gravity compensation, the torque disturbance coming from gravity is appropriately rejected during the arm motion and the tracking accuracy is not disturbed.

C. Payload estimation

To show the payload estimation capability of the approach illustrated in Section V-C, we attached a $5kg$ mass to the arm tip. To discard high frequency disturbances from the estimation the output m_p of the estimator, which is recomputed at each control loop a 1st order butterworth filter with 1 Hz cut-off frequency. In Fig. 10 we show the estimation for the mass added at time $3.75s$. The estimation error is approximately equal to $0.5kg$.

D. Walking tests with arm

We performed walking test with arm moving to verify both the mobile platform and arm controller capability. The enclosed video (see Section VIII) shows the walking experimental results with static and moving arm. We had to keep the walking velocity slow because the hip joints were very close to the torque limits. Furthermore, the mobile platform was not originally designed to carry such big unbalanced load in the front.

VII. Conclusion and Future Work

In this paper, we proposed an attachment configuration for the arm with multi-legged robot to provide a uniform workspace in front, below and above the base robot (HyQ). We presented a control framework that integrate a mobile-platform controller and a robust model-free arm controller combined with payload estimation module. The mobile-platform controller ensure tracking the CoM position and trunk orientation while optimizing for the ground reaction forces and compensating for unbalanced loads and disturbances coming from of the arm. The model-free arm controller compensates for disturbances and tracks the desired trajectory robustly to manipulate objects. The integrated payload estimator module is used to estimate unknown payload carries by manipulator to update the robot CoM location and ensure balance of the mobile platform. We verified and shown the effectiveness of this control framework in simulation and real-world experiments. The future work will mainly focus on extending the arm controller and combining it with the mobile controller. The arm controller will be extended to achieve active impedance behaviour. It will allow the manipulator to be complaint when interacting with the environment but stiff otherwise. The arm will no longer be considered as separated from the controller of the legs. The arm joints will be incorporated in the optimization as if it was a fifth leg, and the end-effector force will be controlled in a similar fashion as the foot contact forces.

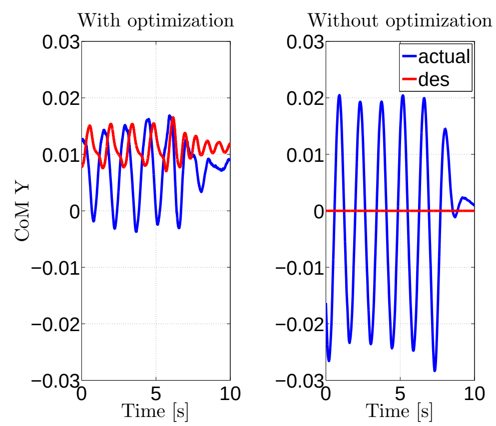

Fig. 8. Rejection of arm motion disturbances at $0.7Hz$, on the robot CoM with and without the mobile platform controller. Blue line represent the actual COM $Y[m]$ position. Whereas, the red line represent desired COM $Y[m]$ position.

VIII. Appendix

The youtube link of real robot experiments: `https://youtu.be/RKwWxEc-ric`

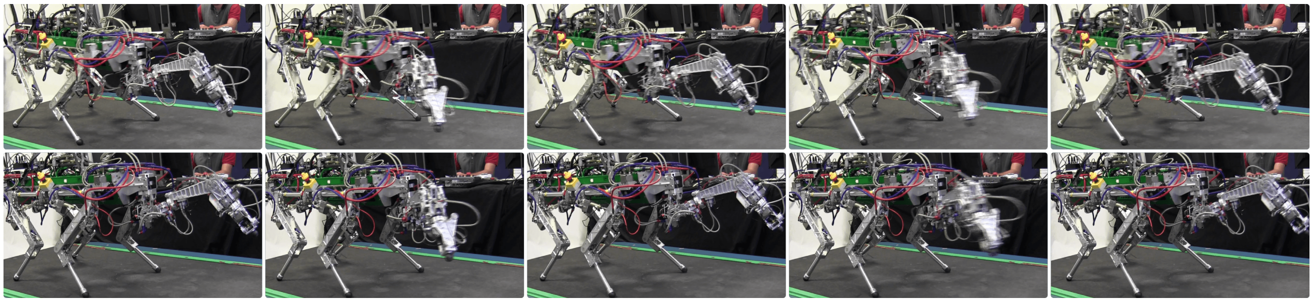

Fig. 7. Snapshots of the two experimental trials used to evaluate the performance of our framework. From top to bottom: Static tests with moving arm without (first row) and with (second row) mobile platform controller.

TABLE II

ROOT-MEAN-SQUARE (RMS) VALUE OF PEAK TO PEAK OSCILLATION ON COM Y $[m]$ DUE TO ARM MOTION AT DIFFERENT FREQUENCIES

Frequencies	With optimization	Without optimization
0.5Hz	0.0058	0.0141
0.6Hz	0.0060	0.0142
0.7Hz	0.0070	0.0144

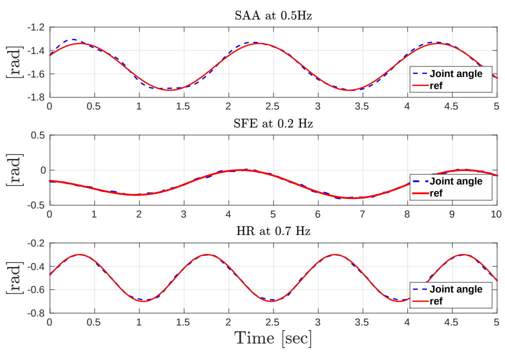

Fig. 9. The first three shoulder joints position tracking: the blue dotted line represent the result of time delay controller and the red solid line represent the desired trajectory.

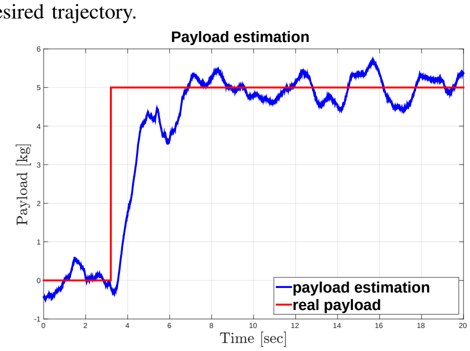

Fig. 10. Estimation of a $5kg$ payload at the end-effector.

REFERENCES

[1] C. Semini, N. G. Tsagarakis, E. Guglielmino, M. Focchi, F. Cannella, and D. G. Caldwell, "Design of HyQ - a hydraulically and electrically actuated quadruped robot," *IMechE Part I: Journal of Systems and Control Engineering*, vol. 225, no. 6, pp. 831–849, 2011.

[2] V. Barasuol, J. Buchli, V. J. D. Negri, E. R. D. Pieri, D. G. Caldwell, and C. Semini, "On trajectory generation and active impedance for running trotting," in *Dynamic Walking*, 2014.

[3] A. Winkler, I. Havoutis, S. Bazeille, J. Ortiz, M. Focchi, D. G. Caldwell, and C. Semini, "Path planning with force-based foothold adaptation and virtual model control for torque controlled quadruped robots," in *IEEE International Conference on Robotics and Automation (ICRA)*, 2014.

[4] B. U. Rehman, M. Focchi, M. Frigerio, J. Goldsmith, D. G. Caldwell, and C. Semini, "Design of a hydraulically actuated arm for a quadruped robot," in *Proceedings of the International Conference on Climbing and Walking Robots (CLAWAR)*, 2015.

[5] A. Junichi, I. Mineo, N. Takashi, and A. Asamu, "Field test of aquatic walking robot for underwater inspection," in *Proceedings of the 7th ISARC, Bristol, United Kingdom*, 1990.

[6] "http://www.hitachi.co.jp/rd/portal/research/robotics/history/1990.html."

[7] K. Munsang, K. Sungchul, L. Sooyong, C. Woojin, C. Kyoungrae, and L. Chong-Won, "Development of a humanoid robot centaur-design, human interface, planning and control of its upper-body," in *Systems, Man, and Cybernetics, 1999. IEEE SMC '99 Conference Proceedings*, 1999.

[8] S. Tsuda, K. Shinozaki, and R. Nakatsu, "Development and evaluation of a centaur robot," in *Service Robotics and Mechatronics, Springer*, 2010.

[9] A. Halme, v. Koskinen, V.-P. Aarnio, S. Salmi, I. Leppnen, and S. Ylnen, "Workpartner - future interactive servicerobot," in *In Proceedings of the 9th Finnish Artificial Intelligence Conference*, 2000.

[10] J. Stückler, M. Schwarz, M. Schadler, A. Topalidou-Kyniazopoulou, and S. Behnke, "Nimbro explorer: Semi-autonomous exploration and mobile manipulation in rough terrain," in *Journal of Feild Robotics, Wiley*, 2015.

[11] A. Roennau, G. Heppner, L. Pfotzer, and D. R., "Lauron v: Optimized leg configuration for the design of a bio-inspired walking robot," in *in the proceedings of international conference on climbing and walking robots (CLAWAR)*, 2013.

[12] Y. Abe, B. Stephens, M. P. Murphy, and A. A. Rizzi, "Dynamic whole-body robotic manipulation," in *Proc. SPIE 8741, Unmanned Systems Technology*, 2013.

[13] M. Hutter, P. Leemann, S. Stevsiic, A. Michel, D. Jud, M. A. Hoepflinger, R. Y. Siegwart, R. Figi, C. Caduff, M. Loher, and S. Tagmann, "Towards optimal force distribution for walking excavators," in *International Conference on Advanced Robotics (ICAR)*, 2015.

[14] D. E. Orin, A. Goswami, and S.-H. Lee, "Centroidal dynamics of a humanoid robot," *Autonomous Robots*, vol. 35, pp. 161–176, June 2013.

[15] M. Focchi, A. Del Prete, I. Havoutis, R. Featherstone, D. Caldwell, and C. Semini, "High-slope Terrain Locomotion for Torque-Controlled Quadruped Robots," tech. rep., 2015.

[16] C. Ott, M. a. Roa, and G. Hirzinger, "Posture and balance control for biped robots based on contact force optimization," *2011 11th IEEE-RAS International Conference on Humanoid Robots*, pp. 26–33, Oct. 2011.

[17] T. Boaventura, C. Semini, J. Buchli, M. Frigerio, M. Focchi, and D. G. Caldwell, "Dynamic torque control of a hydraulic quadruped robot," *2012 IEEE International Conference on Robotics and Automation*, pp. 1889–1894, May 2012.

[18] R. Featherstone, *Rigid Body Dynamics Algorithms*. Springer, New York, 2007.

[19] J. Lee, H. Dallali, N. Tsagarakis, and D. Caldwell, "Robust and model-free link position tracking control for humanoid coman with multiple compliant joints," in *International Conference on Humanoid Robots (Humanoids),*, 2013.

[20] K. Youcef-Toumi and S.-T. Wu, "Input/output linearization using time delay control," *Journal of dynamic systems, measurement, and control*, vol. 114, no. 1, pp. 10–19, 1992.

[21] T. Hsia and L. Gao, "Robot manipulator control using decentralized linear time-invariant time-delayed joint controllers," in *IEEE Int. Conf. Robotics and Automation*, pp. 2070–2075, IEEE, 1990.